Conjugate symmetric sequency-ordered complex Hadamard transform

Aung, Aye; Ng, Boon Poh; Rahardja, Susanto

2009

Aung, A., Ng, B. P., & Rahardja, S. (2009). Conjugate Symmetric Sequency-Ordered Complex Hadamard Transform. IEEE Transactions on Signal Processing, 57(7), 2582-2593.

https://hdl.handle.net/10356/93914

https://doi.org/10.1109/TSP.2009.2017572

Conjugate Symmetric Sequency-Ordered Complex Hadamard Transform

Aye Aung, Boon Poh Ng and Susanto Rahardja

***Abstract*—A new transform known as conjugate symmetric sequency-ordered complex Hadamard transform (CS-SCHT) is presented in this paper. The transform matrix of this transform possesses sequency ordering and the spectrum obtained by the CS-SCHT is conjugate symmetric. Some of its important properties are discussed and analyzed. Sequency defined in the CS-SCHT is interpreted as compared to frequency in the discrete Fourier transform. The exponential form of the CS-SCHT is derived, and the proof of the dyadic shift invariant property of the CS-SCHT is also given. The fast and efficient algorithm to compute the CS-SCHT is developed using the sparse matrix factorization method and its computational load is examined as compared to that of the SCHT. The applications of the CS-SCHT in spectrum estimation and image compression are discussed. The simulation results reveal that the CS-SCHT is promising to be employed in such applications.**

***Index Terms*—Complex Hadamard transforms, discrete orthogonal transforms, fast algorithms, dyadic shift invariant, conjugate symmetric sequency-ordered complex Hadamard transform (CS-SCHT).**

I. Introduction

THE Hadamard transform has been considered widely as a practical tool to process signals, especially in the areas of digital signal and image processing, filtering, communications and digital logic design [1]–[9] due to its simple implementation with the use of fast algorithms. It is known from the literature that the Walsh functions can be arranged to form any of three main orderings which are in common use. They are the Walsh or sequency order, dyadic order and natural or Hadamard order [10], [11]. The choice of orderings depends on the particular applications [12]. Since, the row vectors of a Hadamard matrix are simply the sampled versions of the Walsh functions, the ordering of Hadamard transforms describes the sequence in which the Walsh functions are positioned in the transform matrix. For instance, the Walsh Hadamard transform (WHT) matrix simply expresses that a sampled Walsh function series is arranged in natural or Hadamard order. If the Walsh function values are arranged in ascending values of sequencies in the transform matrix, a sequency-ordered Walsh transform (SOWT) is obtained. In most applications of signal processing, sequency ordering is preferred due to its analogy to frequency in the discrete Fourier transform (DFT) [13], [14].

A set of complex orthogonal transforms known as unified complex Hadamard transforms (UCHTs) is introduced in [15]–[17] for such needs especially employed for multiple-valued logic design, communications and the signal processing applications dealing with complex-valued functions. The transform matrices are confined to four complex integer values $\{\pm 1, \pm j\}$ where $j = \sqrt{-1}$. But the UCHT matrices do not exhibit certain ordering which may correspond to the WHT or the SOWT. Thereafter, sequency-ordered complex Hadamard transform (SCHT) whose transform matrix shows the sequency ordering is introduced in [18] for some particular applications in communications and signal processing. It is a complex Hadamard transform whose row vectors are arranged in an increasing number of sequencies. The SCHT is shown to have certain significance in spectrum estimation as well as in image watermarking. It has also been applied in the direct sequence (DS) CDMA systems [19], in which each row vector of an SCHT matrix is used as a complex spreading sequence to be assigned to a particular user. But the SCHT coefficients are the complex numbers comprised of real and imaginary parts and they are not conjugate symmetric, hence, more memory are needed to store the coefficients for analysis and synthesis in transform implementation. For example, the SCHT may not be suitable to be employed in image compression as it contradicts the goal of reducing bit rate (which implies less transform coefficients to store) for image compression. On the other hand, only half of the spectral coefficients are required for the analysis in the UCHTs with the half spectrum property (HSP) and the DFT (whose spectrum is conjugate symmetric). It is then the purpose of this paper to propose a new version of SCHT called conjugate symmetric sequency-ordered complex Hadamard transform (CS-SCHT for short) whose spectrum is conjugate symmetric, and which is expected to outperform previous introduced SCHT in spectrum estimation. As said, the CS-SCHT spectrum is conjugate symmetric so only half of spectral coefficients are required for synthesis and analysis. This in turn reduces the memory requirement in processing for the applications such as real-time image watermarking and spectrum estimation.

Now let us focus on sequency defined in the SCHT [18]. In fact, sequency of the SCHT is complex sequency which describes the amount of rotations (the number of zero crossings) of each row vector of an SCHT matrix in the unit circle of a complex plane over a normalized time base $0 \leq t \leq 1$. This is analogous to frequency in the DFT if frequency is defined as the number of times that each row vector of a DFT matrix crosses the imaginary axis in the unit circle per unit time interval. In the DFT, however, the term frequency refers to periodic repetition rate of sinusoidal waves as well as the rotation of individual row vector in a DFT matrix in the unit circle. This is because the DFT transform matrix is conjugate symmetric and we can intuitively regroup the row vectors of a

A. Aung and B.P. Ng are with the School of Electrical and Electronic Engineering, Nanyang Technological University, Singapore 639798 (E-mail: aye_aung@pmail.ntu.edu.sg and ebpng@ntu.edu.sg).

S. Rahardja is with the Agency for Science, Technology, and Research (A*STAR), Institute for Infocomm Research, Singapore 138632 (E-mail: rsusanto@i2r.a-star.edu.sg; susantorahardja@ieee.org).

DFT matrix to obtain the corresponding sinusoidal waves with respective frequencies (which is to be explained in Section III). The rotation of each row vector of a DFT matrix in the unit circle and the periodic repetition rate of the corresponding sinusoidal waves are observed to be the same, which defines frequency in the DFT.

In this paper, we introduce the conjugate symmetric version of the SCHT, whose sequency is directly related to frequency of the DFT. The rest of the paper is organized as follows. Section II describes the construction of the CS-SCHT transform matrix based on the conjugate symmetric natural-ordered complex Hadamard transform (CS-NCHT) whose construction is based on the WHT and the direct block matrix operation. The definition of the direct block matrix operator is also given. The interpretation of sequency in the CS-SCHT is presented in Section III. Some important properties of the CS-SCHT are derived and analyzed in Section IV, including the exponential property of the CS-SCHT, the dyadic shift invariant CS-SCHT power spectrum and its proof. Using the sparse matrix factorization approach, a fast algorithm to compute an N-point CS-SCHT is derived in Section V and its computational complexity is examined as compared with that of the SCHT. Some applications of the CS-SCHT are suggested in Section VI together with the supporting simulation results and discussions. Finally, this paper is concluded in Section VII.

II. Basic Definitions of the CS-SCHT

In this section, we shall present the construction of the CS-SCHT matrices. Before going directly to the generation of the CS-SCHT, we first define the direct block matrix operator which is to be used in the subsequent construction.

Let $\mathbf{B}$ be a block matrix such that

$$\mathbf{B} = \begin{bmatrix} \mathbf{B}_{11} & \mathbf{B}_{12} & \cdots & \mathbf{B}_{1N} \\ \mathbf{B}_{21} & \mathbf{B}_{22} & \cdots & \mathbf{B}_{2N} \\ \vdots & \vdots & \ddots & \vdots \\ \mathbf{B}_{M1} & \mathbf{B}_{M2} & \cdots & \mathbf{B}_{MN} \end{bmatrix},$$

$\mathbf{R}$ be a row block matrix, that is,

$$\mathbf{R} = \begin{bmatrix} \mathbf{R}_1 & \mathbf{R}_2 & \cdots & \mathbf{R}_N \end{bmatrix}$$

and $\mathbf{C}$ be a column block matrix which is

$$\mathbf{C} = \begin{bmatrix} \mathbf{C}_1 & \mathbf{C}_2 & \cdots & \mathbf{C}_M \end{bmatrix}^T.$$

Then the direct block matrix operator $\diamond$ is defined as

$$\mathbf{B} \diamond \mathbf{R} = \begin{bmatrix} \mathbf{B}_{11}\mathbf{R}_1 & \mathbf{B}_{12}\mathbf{R}_2 & \cdots & \mathbf{B}_{1N}\mathbf{R}_N \\ \mathbf{B}_{21}\mathbf{R}_1 & \mathbf{B}_{22}\mathbf{R}_2 & \cdots & \mathbf{B}_{2N}\mathbf{R}_N \\ \vdots & \vdots & \ddots & \vdots \\ \mathbf{B}_{M1}\mathbf{R}_1 & \mathbf{B}_{M2}\mathbf{R}_2 & \cdots & \mathbf{B}_{MN}\mathbf{R}_N \end{bmatrix} \quad (1)$$

and

$$\mathbf{B} \diamond \mathbf{C} = \begin{bmatrix} \mathbf{B}_{11}\mathbf{C}_1 & \mathbf{B}_{12}\mathbf{C}_1 & \cdots & \mathbf{B}_{1N}\mathbf{C}_1 \\ \mathbf{B}_{21}\mathbf{C}_2 & \mathbf{B}_{22}\mathbf{C}_2 & \cdots & \mathbf{B}_{2N}\mathbf{C}_2 \\ \vdots & \vdots & \ddots & \vdots \\ \mathbf{B}_{M1}\mathbf{C}_M & \mathbf{B}_{M2}\mathbf{C}_M & \cdots & \mathbf{B}_{MN}\mathbf{C}_M \end{bmatrix} \quad (2)$$

where the submatrices $\mathbf{B}_{mn}, \mathbf{R}_k$ and $\mathbf{C}_l$ are the square matrices which have the same dimensions, and m, n, k and l are positive integers such that $1 \le m, l \le M$ and $1 \le n, k \le N$. If the dimensions of the submatrices are 1×1, the operation of the direct block matrix operator is equivalent to that of the matrix operator defined in [15].

Now we first define the CS-NCHT based on the WHT and the direct block matrix operator as the CS-SCHT is a bit-reversed version of the CS-NCHT. Hence, the generation of the CS-SCHT is different from that of the SCHT where the SCHT is constructed based on the complex Rademacher matrices [18]. Let $\boldsymbol{\mathcal{H}}_N$ be any CS-NCHT matrix of dimension $N \times N$ where $N = 2^n$. Then, it is a square matrix defined as

$$\boldsymbol{\mathcal{H}}_N = \left[\begin{array}{c|c} \boldsymbol{\mathcal{H}}_{N/2} & \boldsymbol{\mathcal{H}}_{N/2} \\ \hline \boldsymbol{\mathcal{H}}'_{N/2}\mathbf{S}_{N/2} & -\boldsymbol{\mathcal{H}}'_{N/2}\mathbf{S}_{N/2} \end{array}\right] \quad (3)$$

where

$$\mathbf{S}_{2^{n-1}} = \begin{bmatrix} \mathbf{I}_{2^{n-2}} & \mathbf{0} \\ \mathbf{0} & j\mathbf{I}_{2^{n-2}} \end{bmatrix} \quad (4)$$

and $\boldsymbol{\mathcal{H}}'_{N/2}$ is a real Hadamard matrix whose rows are arranged in a certain manner and it is defined recursively as

$$\boldsymbol{\mathcal{H}}'_{N/2} = \left[\begin{array}{c|c} \boldsymbol{\mathcal{H}}'_{N/4} & \boldsymbol{\mathcal{H}}'_{N/4} \\ \hline \boldsymbol{\mathcal{H}}'_{N/4}\mathbf{I}'_{N/4} & -\boldsymbol{\mathcal{H}}'_{N/4}\mathbf{I}'_{N/4} \end{array}\right] \quad (5)$$

where $(N/4) = 2^{n-2}$,

$$\mathbf{I}'_{2^{n-2}} = \begin{bmatrix} \mathbf{I}_{2^{n-3}} & \mathbf{0} \\ \mathbf{0} & -\mathbf{I}_{2^{n-3}} \end{bmatrix} \quad (6)$$

is the identity matrix of size $2^{n-2} \times 2^{n-2}$ where the bottom half of the elements are multiplied by (-1). Consequently, $\boldsymbol{\mathcal{H}}_{N/2}$ and $\boldsymbol{\mathcal{H}}'_{N/2}$ can be further reduced to the dimension of 2×2, which is defined as

$$\boldsymbol{\mathcal{H}}'_2 = \boldsymbol{\mathcal{H}}_2 = \begin{bmatrix} 1 & 1 \\ 1 & -1 \end{bmatrix}.$$

In this way, an $N \times N$ CS-NCHT matrix can be expressed using the CS-NCHT matrices of order $(N/2) \times (N/2)$, and the smallest dimension of the CS-NCHT matrix will be the size of 4×4 as shown below.

$$\boldsymbol{\mathcal{H}}_4 = \left[\begin{array}{c|c} \boldsymbol{\mathcal{H}}_2 & \boldsymbol{\mathcal{H}}_2 \\ \hline \boldsymbol{\mathcal{H}}'_2\mathbf{S}_2 & -\boldsymbol{\mathcal{H}}'_2\mathbf{S}_2 \end{array}\right] = \begin{bmatrix} 1 & 1 & 1 & 1 \\ 1 & -1 & 1 & -1 \\ 1 & j & -1 & -j \\ 1 & -j & -1 & j \end{bmatrix}. \quad (7)$$

As a result, any CS-NCHT matrix of dimension $N \times N$ can be defined using the WHT matrix and the direct block matrix operator as follows:

$$\boldsymbol{\mathcal{H}}_N = \mathbf{W}_N \diamond \mathbf{A}'_{n-1,n-1} \diamond \cdots \diamond \mathbf{A}'_{2,2} \diamond \mathbf{A}_{1,1} \quad (8)$$

where $N = 2^n$, $\mathbf{W}_N$ is the $N \times N$ WHT matrix,

$$\begin{aligned} \mathbf{A}_{1,1} &= [\mathbf{I}_{2^{n-1}}, \mathbf{S}_{2^{n-1}}]^T \\ \mathbf{A}'_{2,2} &= [\mathbf{I}_{2^{n-2}}, \mathbf{S}_{2^{n-2}}, \mathbf{I}_{2^{n-2}}, \mathbf{I}'_{2^{n-2}}]^T \\ &\vdots \\ \mathbf{A}'_{n-1,n-1} &= [\mathbf{I}_2, \mathbf{S}_2, \mathbf{I}_2, \mathbf{I}'_2, \cdots, \mathbf{I}_2, \mathbf{I}'_2]^T \end{aligned} \quad (9)$$

where $(\cdot)^T$ represents the transpose, and $\diamond$ denotes the direct block matrix operator which was previously defined.

Let us, for example, consider $N = 8$. Then, $n = \log_2 8 = 3$ and (8) becomes

$$\boldsymbol{\mathcal{H}}_8 = \mathbf{W}_8 \diamond \mathbf{A}'_{2,2} \diamond \mathbf{A}_{1,1}. \tag{10}$$

Substituting the corresponding values defined in (9) into (10), we have

$$\boldsymbol{\mathcal{H}}_8 = \left[\begin{array}{cc|cc} \mathbf{W}_2 & \mathbf{W}_2 & \mathbf{W}_2 & \mathbf{W}_2 \\ \mathbf{W}_2 & -\mathbf{W}_2 & \mathbf{W}_2 & -\mathbf{W}_2 \\ \hline \mathbf{W}_2 & \mathbf{W}_2 & -\mathbf{W}_2 & -\mathbf{W}_2 \\ \mathbf{W}_2 & -\mathbf{W}_2 & -\mathbf{W}_2 & \mathbf{W}_2 \end{array}\right] \diamond \begin{bmatrix} \mathbf{I}_2 \\ \mathbf{S}_2 \\ \mathbf{I}_2 \\ \mathbf{I}'_2 \end{bmatrix} \diamond \begin{bmatrix} \mathbf{I}_4 \\ \mathbf{S}_4 \end{bmatrix} \tag{11}$$

where $\mathbf{W}_2 = \begin{bmatrix} 1 & 1 \\ 1 & -1 \end{bmatrix}$ is the 2×2 WHT matrix. Therefore,

$$\boldsymbol{\mathcal{H}}_8 = \begin{bmatrix} 1 & 1 & 1 & 1 & 1 & 1 & 1 & 1 \\ 1 & -1 & 1 & -1 & 1 & -1 & 1 & -1 \\ 1 & j & -1 & -j & 1 & j & -1 & -j \\ 1 & -j & -1 & j & 1 & -j & -1 & j \\ 1 & 1 & j & j & -1 & -1 & -j & -j \\ 1 & -1 & j & -j & -1 & 1 & -j & j \\ 1 & -1 & -j & j & -1 & 1 & j & -j \\ 1 & 1 & -j & -j & -1 & -1 & j & j \end{bmatrix}. \tag{12}$$

As such any CS-NCHT matrix of dimension $N \times N$ where $N = 2^n$ can be achieved. Having defined the CS-NCHT, a CS-SCHT matrix can be obtained from a CS-NCHT matrix through a bit reversal conversion and vice versa. Let $\mathbf{H}_N$ be any CS-SCHT matrix of size $N \times N$. Then it is defined as

$$\mathbf{H}_N(p,k) = \boldsymbol{\mathcal{H}}_N(b(p),k) \tag{13}$$

where p and k are the row and column indices of a matrix such that $0 \le p,k \le N-1$ and $b(p)$ is the decimal number obtained by the bit-reversed operation of the decimal p. As an example, $\mathbf{H}_8$ is obtained as

$$\mathbf{H}_8 = \begin{bmatrix} \mathbf{H}_8(0,k) \\ \mathbf{H}_8(1,k) \\ \mathbf{H}_8(2,k) \\ \mathbf{H}_8(3,k) \\ \mathbf{H}_8(4,k) \\ \mathbf{H}_8(5,k) \\ \mathbf{H}_8(6,k) \\ \mathbf{H}_8(7,k) \end{bmatrix} = \begin{bmatrix} \boldsymbol{\mathcal{H}}_8(0,k) \\ \boldsymbol{\mathcal{H}}_8(4,k) \\ \boldsymbol{\mathcal{H}}_8(2,k) \\ \boldsymbol{\mathcal{H}}_8(6,k) \\ \boldsymbol{\mathcal{H}}_8(1,k) \\ \boldsymbol{\mathcal{H}}_8(5,k) \\ \boldsymbol{\mathcal{H}}_8(3,k) \\ \boldsymbol{\mathcal{H}}_8(7,k) \end{bmatrix} \tag{14}$$

in which the row vectors of the matrix are arranged in increasing order of zero crossings in the unit circle of a complex plane. Besides, the pth row of the matrix is the conjugate of the $(N-p)$th row vector where $p = 1, 2, \ldots, (N/2)-1$ and $N = 2^n$, hence, the spectrum obtained by using this matrix is shown to be conjugate-symmetric. The 0th and $(N/2)$th row vectors correspond to the DC and Nyquist frequency components in the DFT matrix, respectively. As such any CS-SCHT matrix of dimension $N \times N$ can be generated. This completes the construction of the CS-SCHT. Having developed the CS-SCHT matrix, the CS-SCHT of an N-point complex signal vector $\mathbf{x}_N = [x(0), x(1), \ldots, x(N-1)]^T$ is defined as

$$\mathbf{X}_N = \frac{1}{N}\overline{\mathbf{H}}_N \mathbf{x}_N \tag{15}$$

where $\mathbf{X}_N = [X(0), X(1), \cdots, X(N-1)]^T$ is the transformed complex column vector, $\overline{(\cdot)}$ denotes the complex conjugate and $\mathbf{H}_N$ is the CS-SCHT matrix as defined in (13). The data sequence can be uniquely recovered from the inverse transform, that is,

$$\mathbf{x}_N = \mathbf{H}_N^T \mathbf{X}_N \tag{16}$$

since $\mathbf{H}_N^T \overline{\mathbf{H}}_N = \mathbf{H}_N^* \mathbf{H}_N = N\mathbf{I}_N$ (unitary property) where $(\cdot)^*$ represents the complex conjugate transpose.

III. Interpretation of Sequency

The complex Hadamard matrix generated in (13) exhibits sequency ordering, that is, the row vectors of the CS-SCHT matrix are positioned in an ascending order of sequencies. Sequency is defined as one half of the average number of zero crossings per unit time in the unit circle of a complex plane [11], [13]. As indicated earlier, sequency in the CS-SCHT is analogous to frequency in the DFT. Since the CS-SCHT matrix of dimension $N \times N$ where $N = 2^n$ is conjugate symmetric, we can intuitively separate the real and imaginary terms and regroup them as in the DFT to obtain the corresponding waveforms (which is an approximation of the sinusoidal waves). This process is illustrated below. The new real matrix obtained from the $N \times N$ CS-SCHT matrix is denoted as $\mathbf{H}_{R,N}$ and

$$\mathbf{H}_{R,N} = \begin{bmatrix} \mathbf{H}_N(0,k) \\ \frac{1}{2}(\Im\{\mathbf{H}_N(1,k)\} - \Im\{\mathbf{H}_N(N-1,k)\}) \\ \frac{1}{2}(\Re\{\mathbf{H}_N(1,k)\} + \Re\{\mathbf{H}_N(N-1,k)\}) \\ \frac{1}{2}(\Im\{\mathbf{H}_N(2,k)\} - \Im\{\mathbf{H}_N(N-2,k)\}) \\ \vdots \\ \frac{1}{2}\left(\Im\left\{\mathbf{H}_N(\frac{N}{2}-1,k)\right\} - \Im\left\{\mathbf{H}_N(\frac{N}{2}+1,k)\right\}\right) \\ \frac{1}{2}\left(\Re\left\{\mathbf{H}_N(\frac{N}{2}-1,k)\right\} + \Im\left\{\mathbf{H}_N(\frac{N}{2}+1,k)\right\}\right) \\ \mathbf{H}_N(\frac{N}{2},k) \end{bmatrix} \tag{17}$$

Considering $N = 8$ as an example, $\mathbf{H}_{R,8}$ is obtained as

$$\begin{aligned} \mathbf{H}_{R,8} &= \begin{bmatrix} \mathbf{H}_8(0,k) \\ \frac{1}{2}(\Im\{\mathbf{H}_8(1,k)\} - \Im\{\mathbf{H}_8(7,k)\}) \\ \frac{1}{2}(\Re\{\mathbf{H}_8(1,k)\} + \Re\{\mathbf{H}_8(7,k)\}) \\ \frac{1}{2}(\Im\{\mathbf{H}_8(2,k)\} - \Im\{\mathbf{H}_8(6,k)\}) \\ \frac{1}{2}(\Re\{\mathbf{H}_8(2,k)\} + \Re\{\mathbf{H}_8(6,k)\}) \\ \frac{1}{2}(\Im\{\mathbf{H}_8(3,k)\} - \Im\{\mathbf{H}_8(5,k)\}) \\ \frac{1}{2}(\Re\{\mathbf{H}_8(3,k)\} + \Im\{\mathbf{H}_8(5,k)\}) \\ \mathbf{H}_8(4,k) \end{bmatrix} \\ &= \begin{bmatrix} 1 & 1 & 1 & 1 & 1 & 1 & 1 & 1 \\ 0 & 0 & 1 & 1 & 0 & 0 & -1 & -1 \\ 1 & 1 & 0 & 0 & -1 & -1 & 0 & 0 \\ 0 & 1 & 0 & -1 & 0 & 1 & 0 & -1 \\ 1 & 0 & -1 & 0 & 1 & 0 & -1 & 0 \\ 1 & -1 & 0 & 0 & -1 & 1 & 0 & 0 \\ 0 & 0 & -1 & 1 & 0 & 0 & 1 & -1 \\ 1 & -1 & 1 & -1 & 1 & -1 & 1 & -1 \end{bmatrix} \end{aligned} \tag{18}$$

where $\mathbf{H}_8$ is the CS-SCHT matrix of size 8×8, $\Re\{\cdot\}$ and $\Im\{\cdot\}$ represent real and imaginary parts of a complex number, respectively. The waveforms which are relevant to

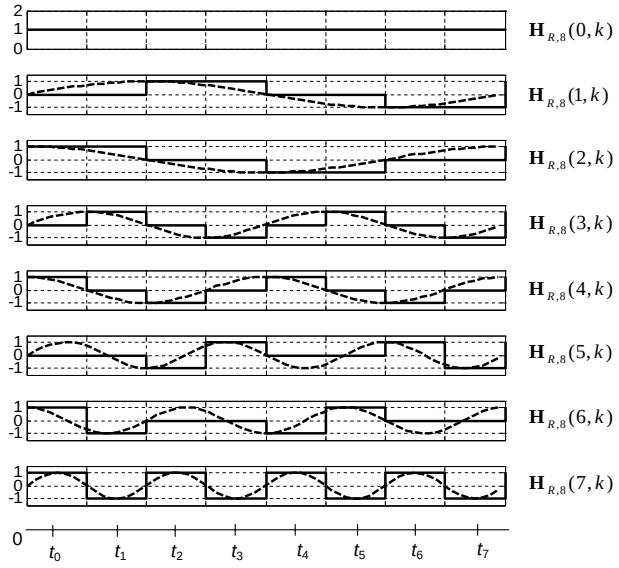

Fig. 1: Approximation of the sinusoidal waves in the DFT using the corresponding waveforms from the CS-SCHT.

each row vector of (18) are shown in Fig. 1 together with the corresponding sinusoidal waveforms from the DFT. It can be seen from the figure that the CS-SCHT is an approximation of sine and cosine waveforms in the DFT by using the pertinent staircase waveforms. Sequency can be expressed as periodic repetition rate of the approximated waveforms as in the case of the DFT where frequency indicates the periodic repetition rate of sinusoidal waveforms. Besides, sequency in the CS-SCHT also satisfies the previous definition which is one half of the average number of zero crossings of each row vector of a matrix in the unit circle of a complex plane per unit time interval. For example, sequency of the pth row vector of a CS-SCHT matrix is p as the number of zero crossings is $2p$. Since the pth and $(N-p)$th row vectors of the CS-SCHT matrices where $p = 1, 2, \ldots, (N/2)-1$ are conjugate-symmetric, they represent the same sequency except that they have different directions of rotations in the unit circle, i.e., clockwise and anti-clockwise directions. This is closely related to frequency in the DFT in which positive frequency and negative frequency (which correspond to the conjugate-symmetric row vectors in the DFT matrix) rotate in oppositive directions as well. It is observed that the phase shifts are not the same each time the row vector of a CS-SCHT matrix rotates in the unit circle, however, the total phase shifts of each row vector of the CS-SCHT matrix are the same as that of the DFT matrix having the same dimension. It should be noted that frequency can be regarded as a special measure of sequency applicable to the sinusoidal waveforms only.

IV. Properties of the CS-SCHT

In this section, we shall present the properties of the CS-SCHT.

Property 1: Exponential Property of the CS-SCHT. Let $h(p,k)$ be the element at the pth row and kth column of any CS-SCHT matrix of dimension $N \times N$ where $N = 2^n$ and $0 \le p, k \le N-1$. Then,

$$h(p,k) = (-1)^{\sum_{r=0}^{n-1} g_r k_r} (-j)^{\sum_{r=0}^{n-1} f_r k_r} \tag{19}$$

where $n = \log_2 N$ and k_r is the rth bit of the binary representation of the decimal integer k, i.e., $(k)_{10} = (k_{n-1}, k_{n-2}, \ldots, k_0)_2$. Besides, g_r is defined to be the rth bit of the binary Gray code [11] of bit reversal representation of the decimal p, and we also define f_r to be the rth bit of the binary bits of the highest power of 2 in $b(p)/2$ where $b(p)$ is the decimal number obtained through a bit-reversed conversion of the decimal p. The example for $N = 8$ is illustrated in Table I to achieve the binary values for the said notations. The complex conjugate of the CS-SCHT matrix can be generated easily by just changing $-j$ to j in (19).

TABLE I: Binary representations for g_r and f_r.

p	Binary	Bit reversal	g_r	$b(p)$	$b(p)/2$	Highest power of 2	f_r
0	000	000	000	0	0	0	000
1	001	100	110	4	2	2	010
2	010	010	011	2	1	1	001
3	011	110	101	6	3	2	010
4	100	001	001	1	0.5	0	000
5	101	101	111	5	2.5	2	010
6	110	011	010	3	1.5	1	001
7	111	111	100	7	3.5	2	010

Property 2: Unitarity. The CS-SCHT is an orthogonal transform whose row vectors are orthogonal in the complex domain as

$$|\det \mathbf{H}_N| = N^{N/2} \tag{20}$$

and

$$\mathbf{H}_N \mathbf{H}_N^* = \mathbf{H}_N^* \mathbf{H}_N = N\mathbf{I}_N \tag{21}$$

where $\mathbf{H}_N$ symbolizes any CS-SCHT matrix of dimension $N \times N$.

Property 3: Linearity. The CS-SCHT is a linear transformation like the DFT.

Property 4: Parseval's Theorem. The energy of the signal in the time and sequency domains is expressed as

$$\frac{1}{N} \sum_{n=0}^{N-1} |x(n)|^2 = \sum_{k=0}^{N-1} |X(k)|^2 \tag{22}$$

where $X(k)$ represents the CS-SCHT coefficients in the sequency domain and $x(n)$ is the signal in the time domain.

Property 5: Conjugate Symmetry. The spectrum transformed by the CS-SCHT is conjugate-symmetric, i.e., the CS-SCHT coefficients $X(k)$ and $X(N-k)$ are conjugate-symmetric pairs where $k = 1, 2, \ldots, (N/2)-1$.

Property 6: Dyadic Shift Invariant Power Spectrum. Let $h(p,k)$ be any element of a CS-SCHT transformation matrix. Then the transformation is said to be *dyadic shift invariant* (DSI) as [20]

$$h(p, k \oplus m) = \begin{cases} h(p,k) \cdot \overline{h(p,m)}, & \text{if both elements} \\ & \text{are imaginary} \\ h(p,k) \cdot h(p,m), & \text{otherwise} \end{cases} \tag{23}$$

and

$$||h(p,k)||^2 = h(p,k)\cdot\overline{h(p,k)} = 1 \tag{24}$$

where $\oplus$ represents the modulo-2 addition and $h(p,k) \in \{\pm 1, \pm j\}$.

Proof: Let $h(p,k)$ be the (pth, kth) element of any CS-SCHT matrix where $N = 2^n$ and $p,k = 0,1,\ldots,N-1$. From *Property 1*, the exponential form of the CS-SCHT is

$$\begin{aligned} h(p,k) &= (-1)^{\sum_{r=0}^{n-1} g_r k_r}(-j)^{\sum_{r=0}^{n-1} f_r k_r} \\ h(p,k\oplus m) &= (-1)^{\sum_{r=0}^{n-1} g_r (k_r\oplus m_r)}(-j)^{\sum_{r=0}^{n-1} f_r (k_r\oplus m_r)}. \end{aligned} \tag{25}$$

From Table II, the Boolean function $g_r(k_r\oplus m_r)$ is equivalent to the function $g_r k_r \oplus g_r m_r$. Therefore, we have

$$\begin{aligned} h(p,k\oplus m) &= (-1)^{\sum_{r=0}^{n-1} g_r (k_r\oplus m_r)}(-j)^{\sum_{r=0}^{n-1} f_r (k_r\oplus m_r)} \\ &= (-1)^{\sum_{r=0}^{n-1} g_r k_r\oplus g_r m_r}(-j)^{\sum_{r=0}^{n-1} f_r k_r\oplus f_r m_r}. \end{aligned} \tag{26}$$

TABLE II: THE TRUTH TABLE FOR $g_r(k_r\oplus m_r)$ AND $g_r k_r\oplus g_r m_r$.

g_r	k_r	m_r	$k_r\oplus m_r$	$g_r k_r$	$g_r m_r$	$g_r\cdot(k_r\oplus m_r)$	$g_r k_r\oplus g_r m_r$
0	0	0	0	0	0	0	0
0	0	1	1	0	0	0	0
0	1	0	1	0	0	0	0
0	1	1	0	0	0	0	0
1	0	0	0	0	0	0	0
1	0	1	1	0	1	1	1
1	1	0	1	1	0	1	1
1	1	1	0	1	1	0	0

Now let us consider each term contained in (26). Then, from Table III, it can be found that

$$\begin{aligned} (-1)^{\sum_{r=0}^{n-1} g_r k_r\oplus g_r m_r} &= (-1)^{\sum_{r=0}^{n-1} g_r k_r + g_r m_r} \\ &= (-1)^{\sum_{r=0}^{n-1} g_r k_r + \sum_{r=0}^{n-1} g_r m_r} \\ &= (-1)^{\sum_{r=0}^{n-1} g_r k_r}\cdot(-1)^{\sum_{r=0}^{n-1} g_r m_r}. \end{aligned} \tag{27}$$

On the other hand, Table IV shows that the functions $(-j)^{\sum_{r=0}^{n-1} f_r k_r\oplus f_r m_r}$ and $(-j)^{\sum_{r=0}^{n-1} f_r k_r + f_r m_r}$ are not equivalent whenever $f_r = k_r = m_r = 1$. Therefore, it is expressed as

$$\begin{aligned} (-j)^{\sum_{r=0}^{n-1} f_r k_r\oplus f_r m_r} &= (-j)^{f_0 k_0\oplus f_0 m_0}(-j)^{f_1 k_1\oplus f_1 m_1} \\ &\quad\cdots(-j)^{f_{n-1} k_{n-1}\oplus f_{n-1} m_{n-1}} \end{aligned} \tag{28}$$

In order to convert $(b_{1,r}\oplus b_{2,r})$ to $(b_{1,r}+b_{2,r})$, consideration is taken into account only if the two binary operands (i.e., $b_{1,r}$ and $b_{2,r}$) are both equal to one. As indicated in *Property 1*, f_r represents the binary code of highest power of 2 in $b(p)/2$ where $b(p)$ is the bit-reversed converted decimal number. Therefore, it has only one bit of 1 in its binary expression and the rest are 0 (see Table I for an example). $f_r k_r$ in (28)

TABLE III: THE TRUTH TABLE FOR $(-1)^{k_r\oplus m_r}$ AND $(-1)^{k_r+m_r}$.

k_r	m_r	$k_r\oplus m_r$	k_r+m_r	$(-1)^{k_r\oplus m_r}$	$(-1)^{k_r+m_r}$
0	0	0	0	1	1
0	1	1	1	-1	-1
1	0	1	1	-1	-1
1	1	0	2	1	1

TABLE IV: THE TRUTH TABLE FOR $(-j)^{f_r k_r\oplus f_r m_r}$ AND $(-j)^{f_r k_r + f_r m_r}$.

f_r	k_r	m_r	$(-j)^{f_r k_r\oplus f_r m_r}$	$(-j)^{f_r k_r + f_r m_r}$
0	0	0	1	1
0	0	1	1	1
0	1	0	1	1
0	1	1	1	1
1	0	0	1	1
1	0	1	$-j$	$-j$
1	1	0	$-j$	$-j$
1	1	1	1	-1

where $r = 0,1,\ldots,n-1$ has only one bit of 1 in its binary notation. Hence, (28) can be rewritten as

$$\begin{aligned} &(-j)^{\sum_{r=0}^{n-1} f_r k_r\oplus f_r m_r} \\ =\ &(-j)^{f_0 k_0 + f_0 m_0}(-j)^{f_1 k_1 + f_1 m_1}\cdots \\ &(-j)^{f_{n-1} k_{n-1} + f_{n-1} m_{n-1}}(-1)^{f_r k_r m_r} \\ =\ &(-j)^{\sum_{r=0}^{n-1} f_r k_r}\cdot(-j)^{\sum_{r=0}^{n-1} f_r m_r}\cdot(-1)^{\sum_{r=0}^{n-1} f_r k_r m_r}. \end{aligned} \tag{29}$$

The term $(-1)^{\sum_{r=0}^{n-1} f_r k_r m_r}$ is included in the above expression (its value can be $\{\pm 1\}$) considering for the case where $f_r = k_r = m_r = 1$ as shown in Table IV. It is also observed from this expression that whenever $f_r = k_r = m_r = 1$, the corresponding elements $h(p,k)$ and $h(p,m)$ are imaginary and one of them is multiplied with -1, which in fact is similar to the conjugation of that imaginary element. Therefore, this will prove the requirement defined in (23). Finally, substituting (27) and (29) into (26), we obtain

$$\begin{aligned} h(p,k\oplus m) &= (-1)^{\sum_{r=0}^{n-1} g_r k_r}\cdot(-1)^{\sum_{r=0}^{n-1} g_r m_r} \\ &\quad\cdot(-j)^{\sum_{r=0}^{n-1} f_r k_r}\cdot(-j)^{\sum_{r=0}^{n-1} f_r m_r} \\ &\quad\cdot(-1)^{\sum_{r=0}^{n-1} f_r k_r m_r} \\ h(p,k\oplus m) &= \begin{cases} h(p,k)\cdot\overline{h(p,m)}, & \text{if both elements} \\ & \text{are imaginary} \\ h(p,k)\cdot h(p,m), & \text{otherwise} \end{cases} \end{aligned} \tag{30}$$

and also

$$||h(p,k)||^2 = h(p,k)\cdot\overline{h(p,k)} = 1. \tag{31}$$

This completes the proof of (23) and (24). The proof is completed here. It is noted that the power spectrum of a real-valued input signal obtained through the DSI transformation is dyadic shift invariant [20]. Hence, the CS-SCHT power spectrum is also dyadic shift invariant.

V. Fast Algorithm of the CS-SCHT

This section will derive the fast algorithm to compute an N-point CS-SCHT using the matrix factorization method. Since the CS-SCHT is the bit-reversed counterpart of the CS-NCHT, the method applied to the latter is also applicable to the former and vice versa. In this section, we shall present the factorization method of the CS-NCHT matrix, which leads to the fast algorithms for the CS-NCHT as well as the CS-SCHT for which the output is arranged in bit-reversed order. The forward transformation matrix defined in (15) is the conjugate of the CS-SCHT matrix but we start with the factoring of the CS-NCHT matrix to derive the fast algorithm. Let us, for example, consider $N = 8$ to conceptualize the method of factorization. Then, the expression in (3) becomes

$$\boldsymbol{\mathcal{H}}_8 = \left[\begin{array}{c|c} \boldsymbol{\mathcal{H}}_4 & \boldsymbol{\mathcal{H}}_4 \\ \hline \boldsymbol{\mathcal{H}}'_4\mathbf{S}_4 & -\boldsymbol{\mathcal{H}}'_4\mathbf{S}_4 \end{array}\right] \tag{32}$$

where

$$\mathbf{S}_4 = \begin{bmatrix} \mathbf{I}_2 & \mathbf{0} \\ \mathbf{0} & j\mathbf{I}_2 \end{bmatrix} \text{ and } \boldsymbol{\mathcal{H}}'_4 = \left[\begin{array}{c|c} \boldsymbol{\mathcal{H}}_2 & \boldsymbol{\mathcal{H}}_2 \\ \hline \boldsymbol{\mathcal{H}}_2\mathbf{I}'_2 & -\boldsymbol{\mathcal{H}}_2\mathbf{I}'_2 \end{array}\right].$$

Equation (32) can be expressed as

$$\boldsymbol{\mathcal{H}}_8 = \begin{bmatrix} \boldsymbol{\mathcal{H}} & \mathbf{0} \\ \mathbf{0} & \boldsymbol{\mathcal{H}}'_4 \end{bmatrix} \begin{bmatrix} \mathbf{I}_4 & \mathbf{0} \\ \mathbf{0} & \mathbf{S}_4 \end{bmatrix} \begin{bmatrix} \mathbf{I}_4 & \mathbf{I}_4 \\ \mathbf{I}_4 & -\mathbf{I}_4 \end{bmatrix}. \tag{33}$$

Subsequently, $\boldsymbol{\mathcal{H}}_4$ and $\boldsymbol{\mathcal{H}}'_4$ can be further factorized and $\boldsymbol{\mathcal{H}}_8$ becomes

$$\begin{aligned} \boldsymbol{\mathcal{H}}_8 \;=\; & \begin{bmatrix} \boldsymbol{\mathcal{H}}_2 & & & \\ & \boldsymbol{\mathcal{H}}_2 & & \\ & & \boldsymbol{\mathcal{H}}_2 & \\ & & & \boldsymbol{\mathcal{H}}_2 \end{bmatrix} \begin{bmatrix} \mathbf{I}_2 & & & \\ & \mathbf{S}_2 & & \\ & & \mathbf{I}_2 & \\ & & & \mathbf{I}'_2 \end{bmatrix} \cdot \\ & \begin{bmatrix} \mathbf{I}_2 & \mathbf{I}_2 & & \\ \mathbf{I}_2 & -\mathbf{I}_2 & & \\ & & \mathbf{I}_2 & \mathbf{I}_2 \\ & & \mathbf{I}_2 & -\mathbf{I}_2 \end{bmatrix} \begin{bmatrix} \mathbf{I}_4 & \\ & \mathbf{S}_4 \end{bmatrix} \begin{bmatrix} \mathbf{I}_4 & \mathbf{I}_4 \\ \mathbf{I}_4 & -\mathbf{I}_4 \end{bmatrix} \end{aligned} \tag{34}$$

where the blank spaces represent the zero elements,

$$\boldsymbol{\mathcal{H}}_2 = \begin{bmatrix} 1 & 1 \\ 1 & -1 \end{bmatrix}, \; \mathbf{S}_2 = \begin{bmatrix} 1 & 0 \\ 0 & j \end{bmatrix} \text{ and } \mathbf{I}'_2 = \begin{bmatrix} 1 & 0 \\ 0 & -1 \end{bmatrix}.$$

The factorization of $\overline{\boldsymbol{\mathcal{H}}}_8$ can be obtained by just changing j to $-j$ in the $\mathbf{S}$ matrices which are included in (34). This factorization will result in fast forward CS-NCHT algorithm. As mentioned earlier, rearranging the output in a bit-reversed order will provide the CS-SCHT coefficients, which gives rise to the fast forward CS-SCHT algorithm. The decomposition of fast forward CS-SCHT for $N = 8$ is illustrated by the signal flow graph in Fig. 2.

For simplicity, the multiplication by the scaling factor $(1/8)$ is omitted in the figure, which in fact can be computed by the binary shifting operations without needing any arithmetic operations. As shown in Fig. 2, the signal flow graph contains three stages and each stage requires eight addition/subtractions. But a total of $2^0 + 2^1 = 3$ complex multiplications by factor $-j$ is needed for three stages. Therefore, it can be concluded that for an N-point CS-SCHT, the fast algorithm has $n = \log_2 N$ stages and each stage needs N addition/subtractions. In general, the total computational requirements for complex input data are $N \log_2 N$ complex addition/subtractions and

$$2^0 + 2^1 + \cdots + 2^{n-2} = \frac{1 - 2^{n-1}}{1 - 2} = (2^{n-1} - 1) \tag{35}$$

complex multiplications for the trivial twiddle factors $-j$. Compared to fast SCHT algorithm reported in [18], they have the same number of complex addition/subtractions but this presented fast CS-SCHT algorithm requires less trivial complex multiplications than fast SCHT algorithm, that is, $(2^{n-1} - 1)$ for the CS-SCHT and $(N/4)\log_2(N/2) = 2^{n-2}(n-1)$ for the SCHT. The numerical numbers are presented in Table V for the comparison purpose. It can be seen from the table that when n is increased, the difference becomes larger and significant.

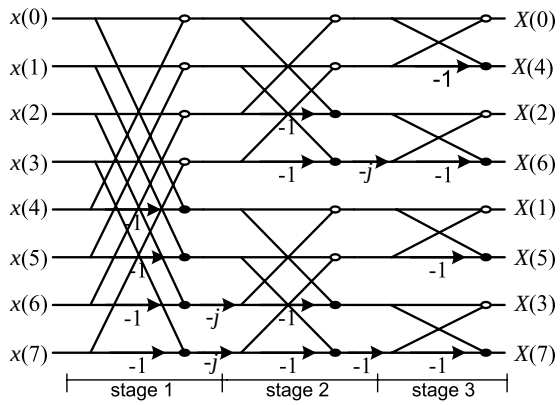

Fig. 2: Signal flow graph illustrating the computation of an 8-point CS-SCHT.

TABLE V: Comparison of computational complexity.

	Number of complex multiplications by the elements $-j$	
n	CS-SCHT	SCHT
3	3	4
4	7	12
5	15	32
6	31	80
7	63	192
8	127	448
9	255	1024
10	511	2304

This fast CS-SCHT algorithm is well suited to adopt the pipelined hardware structure, which was proposed for the SCHT in [21]. The signal flow graph in Fig. 2 is similar to that of the decimation-in-sequency (DIS) fast SCHT algorithm (which was used to develop the pipelined hardware structure for the SCHT) except that the former needs less complex multiplications by the trivial twiddle factors. As pointed out in [21], the operations of swapping and subtraction can be jointly performed with the aid of the $2:1$ complex multiplexers to accomplish the multiplications with $-j$. Therefore, it should be noted that less number of operations are needed to implement the CS-SCHT as compared to the SCHT.

VI. Applications of the CS-SCHT

In this section, we shall present some potential applications of the CS-SCHT including the supporting simulation results.

A. Spectrum Estimation

The CS-SCHT may have certain significance in signal analysis and synthesis due to its sequency ordering and its simple implementation which only requires additions and subtractions for transformation. Fig. 3 illustrates the magnitude response for each row vector of the CS-SCHT matrix for $N = 8$ and Fig. 4 shows the magnitude response for the DFT matrix. It can be seen from the figures that sequency in the CS-SCHT is closely related to frequency in the DFT and the locations of their main lobes are the same even though there are uneven main lobes in the magnitude response of the CS-SCHT as compared to that of the DFT.

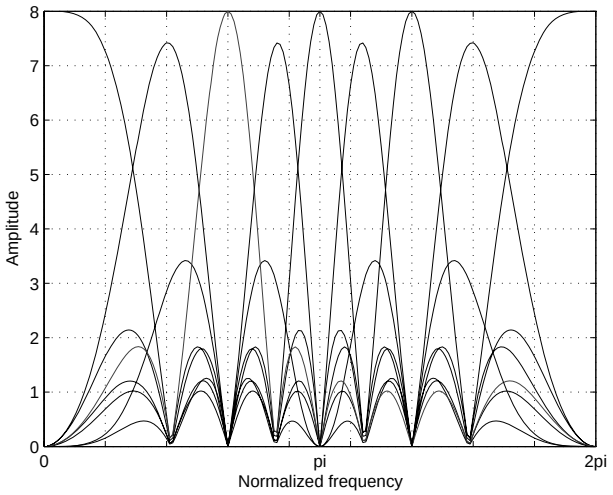

Fig. 3: Magnitude response of the CS-SCHT matrix ($N = 8$).

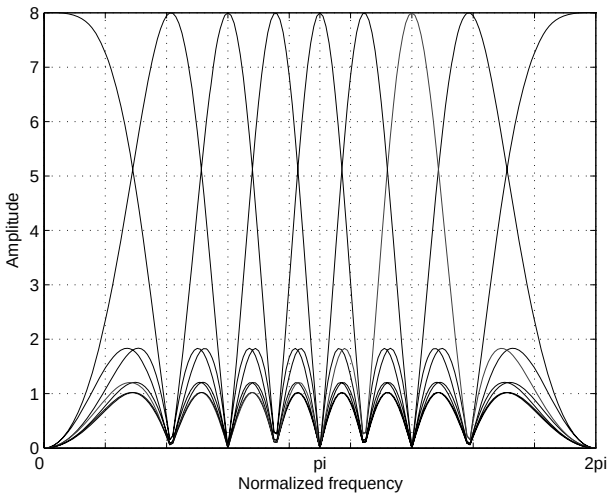

Fig. 4: Magnitude response of the 8×8 DFT matrix.

As an example, the CS-SCHT is applied in spectrum estimation of the sinusoidal waves. Fig. 5 shows the magnitude spectrum of 512-point DFT, CS-SCHT and SCHT of the sinusoidal wave of 1000 Hz using the sampling frequency of 500000 Hz (in order to show the complete spectrum). The corresponding highlighted portion in Fig. 5, which is zoomed in to provide the clear view, is shown in Fig. 6. It can be seen from Fig. 5 that both CS-SCHT and SCHT spectra are closely matched with that of the DFT. The desired main peaks occur in the same locations for all spectra as shown in Fig. 6. But it is observed that the SCHT spectrum has more unwanted side lobes than that of the CS-SCHT as illustrated in the figures. Therefore, it can be concluded that sequency of the CS-SCHT is more closely related to frequency of the DFT than that of the SCHT. Another obvious advantage is that the spectrum obtained by the CS-SCHT are conjugate-symmetric (like the DFT spectrum) as shown in Fig. 5, hence, only half of the spectrum coefficients are required for analysis as compared with the SCHT spectrum. In a nutshell, the CS-SCHT can be considered as a good substitute to replace the DFT in

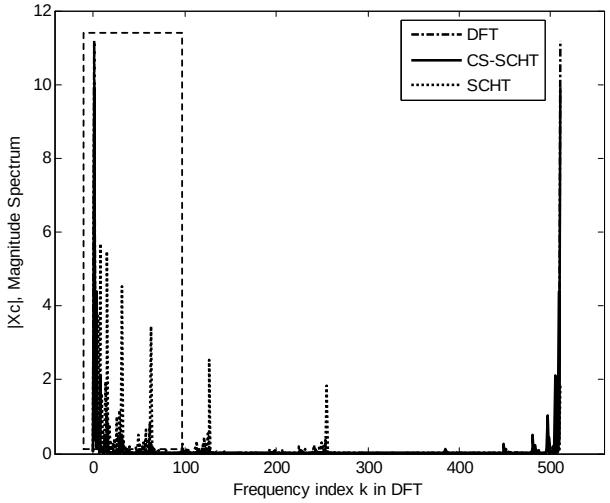

Fig. 5: Magnitude spectra of the DFT, CS-SCHT and SCHT for the sinusoidal wave of 1000 Hz.

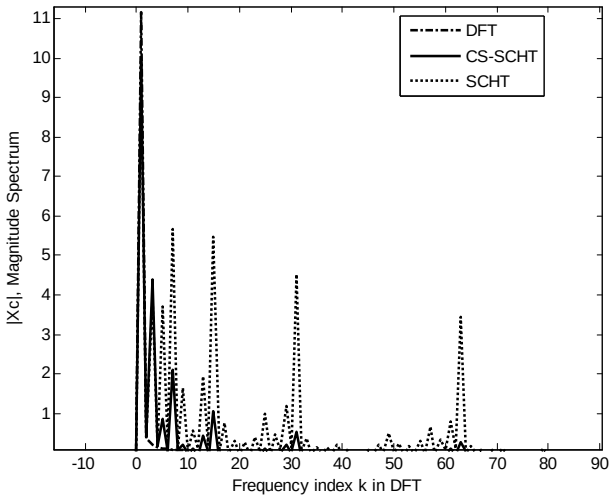

Fig. 6: The highlighted portion in Fig. 5.

spectrum estimation while providing simple implementation and less computational time.

B. Image Compression

Transform coding technique is one of the most popular methods to compress the digital images. In *transform coding*, a linear and reversible transform is used to map the image into a set of transform coefficients which are then quantized and coded. The fundamental goal of image compression is to reduce the bit rate which implies less transform coefficients to reconstruct the image while maintaining an acceptable fidelity or image quality. Therefore, the transforms having good energy compaction property are advisable to be employed in image compression. It is a well-known fact that most orthogonal transforms tend to pack a large fraction of the average energy of the images into a relatively few components of the transform coefficients (energy compaction property) [22]. The most well-known orthogonal transform is the discrete cosine transform (DCT) [11], [22], [23] for its highly information packing capability as well as the availability of various efficient fast computational algorithms [24]. The current standard for compression of still images, JPEG, uses the DCT to compress the images. The WHT [2] is the simplest non-sinusoidal orthogonal transform and also provides comparable performance in image compression as compared with the DCT. It is perhaps a better choice for real-time implementation in some applications.

In this subsection, the CS-SCHT is proposed to be applied in image compression. Since an image can be represented as a matrix consisting of real numbers, real-valued transforms are preferred to be used in order to obtain the real transform coefficients. For this purpose, the 8×8 transform matrix which is derived from the CS-SCHT (shown in (18)) could be used for image compression with very low computational cost, which merely consists of addition/subtractions. Since the CS-SCHT is a complex orthogonal transform, its real-valued transform is also an orthogonal transform. After normalizing the elements of each row vector of (18) by its 2-norm, the 8×8 transform matrix is obtained as

$$\mathbf{C}_8 = \mathbf{D}_8 \cdot \mathbf{H}_{R,8} \tag{36}$$

where $\mathbf{D}_8 = \text{diag}\left\{\sqrt{\frac{1}{8}}, \sqrt{\frac{1}{4}}, \sqrt{\frac{1}{4}}, \sqrt{\frac{1}{4}}, \sqrt{\frac{1}{4}}, \sqrt{\frac{1}{4}}, \sqrt{\frac{1}{4}}, \sqrt{\frac{1}{8}}\right\}$ is the diagonal matrix which consists of the normalization factors. As mentioned in Section III, the row vectors of this matrix are the approximations of the sinusoidal waves in the DFT. Therefore, the input signal can be represented as a linear combination of its row vectors expecting that the signal energy could be concentrated on a few transform coefficients for good compression. The corresponding transform is defined as follows:

$$\mathbf{X}_8 = \mathbf{C}_8 \mathbf{x}_8 \tag{37}$$

where $\mathbf{X}_8 = [X(0), X(1), \ldots, X(7)]^T$ is the transformed column vector and $\mathbf{x}_8 = [x(0), x(1), \ldots, x(7)]^T$ represents the input data vector. The data sequence can be recovered uniquely from the inverse transform, that is,

$$\mathbf{x}_8 = \mathbf{C}_8^T \mathbf{X}_8 \tag{38}$$

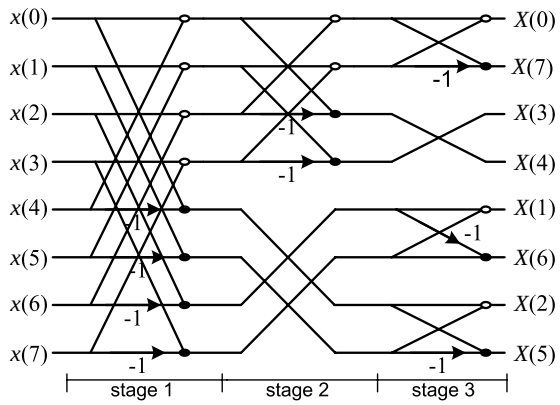

Fig. 7: Signal flow graph of the fast forward algorithm for the real transform derived from the CS-SCHT ($N = 8$).

where $\mathbf{C}_8^T \mathbf{C}_8 = \mathbf{I}_8$ (orthogonal property). The two dimensional (2-D) transform for an 8×8 real image matrix can be obtained by applying 1-D transform on the rows followed by the columns. The resultant transform coefficients are the real numbers, which are suitable for image compression.

The transformation by $\mathbf{C}_8$ can be done efficiently with minimum computational cost by using the fast algorithm. The fast algorithm to compute this transform is derived for the purpose of implementation for image compression. The readers may refer to Appendix for details. The signal flow graph for fast forward 8-point transform is illustrated in Fig. 7. For simplicity, the normalization factors are omitted in the figure, which in fact can be computed after or before the transformation. It can be seen from the figure that only the first stage needs eight addition/subtractions whereas the second and third stages merely requires four and six addition/subtractions, respectively. Therefore, a total of $(8 + 4 + 6) = 18$ addition/subtractions is needed to compute an 8-point 1-D transform. On the other hand, 24 addition/subtractions are required to compute an 8-point traditional fast WHT using the fast algorithm [11]. The same number of multiplications (which is eight) is required for both transforms when the signal is scaled by the normalization factors, which is $\mathbf{D}_8$ mentioned in (36). Hence, an additional savings of $(24 - 18) = 6$ addition/subtractions (which is $\frac{6}{24} \times 100\% = 25\%$) can be gained for one transformation by using the proposed transform as compared to the WHT.

The computer simulations are also conducted to evaluate the mean square error (MSE) performance of the proposed transform for energy compaction property as well as the bit rate (BR) vs peak signal-to-noise ratio (PSNR) performance for image compression. The image block size considered in the simulation is the standard size of 8×8. The original images are divided into non-overlapping 8×8 blocks and the corresponding transforms are performed on these blocks. During the reconstruction process, the coefficients with maximum magnitudes on each transformed 8×8 block are selected based on the compression ratio. Fig. 8 shows the MSE comparison of various transforms based on the 8×8 image blocks with respect to the number of coefficients chosen for reconstructing the Lena image. We have also tested for the Lena image based

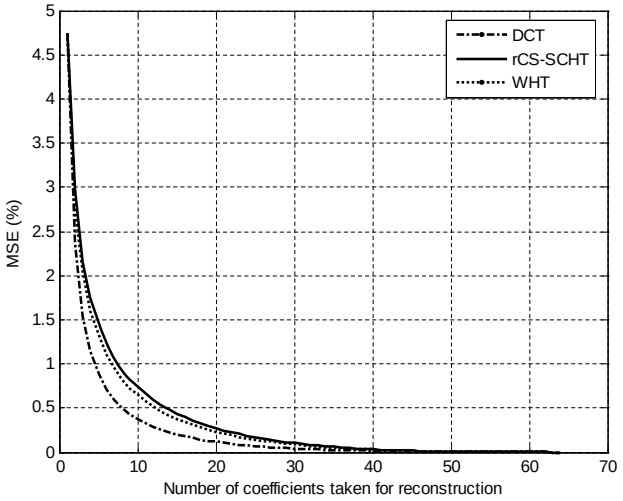

Fig. 8: MSE comparison among the DCT, the proposed transform, and the WHT with respect to the number of coefficients selected during reconstruction for the Lena image.

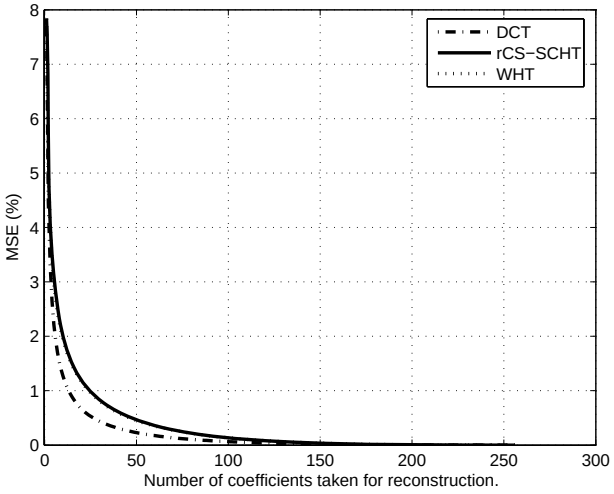

Fig. 9: MSE comparison based on the 16×16 image blocks.

on the 16×16 image blocks and the result is show in Fig. 9. It can be seen from the figures that the MSE performances of the proposed transform and the WHT are comparable to each other for most of the compression ratios (i.e., the number of coefficients selected). Hence, it is observed that the proposed transform also possesses good energy compaction property like the WHT and it is suitable for application in image compression as well.

For image compression, the default settings for the JPEG are used [25] to evaluate the bite rate vs PSNR performance. The test images used in this simulation are the standard Lena and Barbara images. We have tested on other standard images as well and the results are consistent. Table VI lists the comparisons of the PSNR and BR values among the DCT, the proposed transform and the WHT at different values of M (which is the number of transform coefficients selected to reconstruct the original image) for the Lena image. The original Lena image and the respective decompressed images are shown in Fig. 10 with 20 coefficients chosen for reconstruction using different transforms. It is observed from Table VI that when the values of M become larger, the corresponding PSNR values and bit rates are increased for various transforms. That is, more binary bits are required to represent the pixel values of the images with increased values of M, hence, less distortion is occurred to the reconstructed images. Obviously, at any particular value of M, the DCT outperforms the other transforms in terms of PSNR and bit rates at the expense of highly computational cost. On the other hand, it is found from the table that the PSNRs of the reconstructed images and the corresponding bit rates for the proposed transform and the WHT are close to each other at any individual value of M. Besides, their reconstructed image qualities are also equally good enough to compare to that of the DCT as shown in Fig. 10. No significant visual degradation occurs in both images.

TABLE VI: COMPARISONS OF PSNR AND BR AMONG THE DCT, THE PROPOSED TRANSFORM, AND THE WHT FOR THE LENA IMAGE.

	DCT		rCS-SCHT		WHT	
M	PSNR	BR	PSNR	BR	PSNR	BR
8	27.2634	0.5563	24.7848	0.5587	25.6427	0.5562
12	28.1484	0.6480	25.6359	0.6776	26.5533	0.6756
16	29.6632	0.7408	27.3659	0.8103	27.6694	0.7690
20	30.9772	0.8322	28.1081	0.8982	28.3369	0.8526
24	31.1807	0.8864	28.4672	0.9577	28.6208	0.9132
28	31.9008	0.9321	29.2968	1.0211	29.5068	0.9957
32	32.3919	0.9786	30.0928	1.0972	30.3276	1.0468

M - The number of coefficients taken for reconstruction.
BR - Bit rate (bit/pixel).
PSNR - Peak signal-to-noise ratio (dB).

TABLE VII: COMPARISONS AMONG THE TRANSFORMS FOR THE BARBARA IMAGE.

	DCT		rCS-SCHT		WHT	
M	PSNR	BR	PSNR	BR	PSNR	BR
8	26.9354	0.5805	24.7945	0.5812	25.3570	0.5764
12	27.9808	0.6988	25.8175	0.7330	26.5008	0.7287
16	29.0273	0.7976	27.1819	0.8649	27.3502	0.8300
20	29.9303	0.8863	27.7014	0.9602	27.8418	0.9120
24	30.1210	0.9260	28.0872	1.0203	28.1861	0.9623
28	30.6784	0.9805	28.6956	1.0860	28.8896	1.0510
32	31.0625	1.0248	29.2284	1.1500	29.4820	1.1007

But the advantage of the proposed transform over the WHT is the reduced computational cost. As mentioned earlier, an extra savings of 6 addition/subtractions (25%) can be acquired for one transformation by using the proposed transform as compared to the WHT. If an image of 512×512 pixels is considered for image compression, the total number of blocks will be $(512 \times 512) \div (8 \times 8) = 4096$ and each block needs 16 transformations using (37). As one transformation performs 24 addition/subtractions, a total of $24 \times 16 \times 4096 = 1572864$ addition/subtractions is needed for the whole computation if the WHT is used. However, only a total of $1572864 \times 0.75 = 1179648$ addition/subtractions is required for the proposed transform, hence, we can obtain an additional saving

Fig. 10: (a) The original image of Lena, the decompressed images of Lena using (b) the DCT, (c) the proposed transform, and (d) the WHT using 20 transform coefficients.

of $1572864 \times 0.25 = 393216$ addition/subtractions, which is significant in the hardware implementation especially for real-time applications. Therefore, if the hardware savings and simplicity are the first priority to be considered rather than the image quality in the applications, the proposed transform and the WHT are shown to be better choices than the DCT, but among them, the proposed transform is better option to be considered.

Table VII summarizes the comparisons for the Barbara image which contains high frequency components. We have observed from the table that the results are consistent with previous findings concluded for the Lena image.

VII. Conclusion

The conjugate symmetric sequency-ordered complex Hadamard transform is discussed in this paper. It has been shown that sequency defined in the CS-SCHT is more closely related to frequency in the DFT as compared to that of the SCHT. It can be seen that the CS-SCHT is a close approximation to the sinusoidal waves in Fourier analysis using the staircase waveforms while the SOWT provides the approximation of the sine and cosine waves in the DFT using the square waves [26]. As the name follows, the CS-SCHT spectrum of a real-valued data sequence is conjugate-symmetric as well as the transform itself is sequency-ordered and suitable for complex-valued functions, which makes it unique among the transforms. Due to the conjugate-symmetric property, only half of the spectrum are needed for analysis and synthesis, which leads to achieve memory savings in the processing of the transform in the applications as compared to the SCHT.

The construction of the CS-SCHT is based on the CS-NCHT. It has been shown that they can be obtained from the WHT and the direct block matrix operation. Some important properties of the CS-SCHT are discussed and analyzed. The exponential property of the CS-SCHT is mentioned and the definition of dyadic shift invariant property for complex Hadamard transform is given. Subsequently, it has been proved that the power spectrum acquired by the CS-SCHT is dyadic shift invariant. The fast CS-SCHT algorithm is derived using the sparse matrix factorization approach and its computational complexity is examined. It has been investigated that less number of complex multiplications by the trivial twiddle factors, i.e., $-j$ are required to compute an N-point CS-SCHT as compared to that of the SCHT using the fast algorithm. Therefore, less number of swapping and subtraction operations are required when implementing the transform in the pipelined hardware structure [21]. The applications of the CS-SCHT in spectrum estimation and image compression are also mentioned in this paper. The CS-SCHT has been shown to be a better choice to replace the DFT (at the cost of some loss in accuracy of estimation) in signal analysis and synthesis as compared to the SCHT with simple implementation and less computational complexity. Moreover, the new transform which is derived from the CS-SCHT is proposed in image compression. The fast algorithm to compute the 8-point proposed transform is also derived especially for use in image compression. It has been found that the PSNR values of the reconstructed images with respect to the original image using the proposed transform are comparable to that of the WHT at any chosen value of M, the number of coefficients selected. Their corresponding bit rates are also close to each other. But the proposed transform requires less number of addition/subtractions with the use of the presented fast algorithm as compared to that of the WHT. Therefore, the proposed transform have been shown to be better alternative to substitute the DCT in image compression if simplicity and computational cost are the important factors to be considered in the applications.

Appendix

Fast Algorithm for a Real Transform Derived from the CS-SCHT

From (37), the transform is given by

$$\mathbf{X}_8 = \mathbf{C}_8 \mathbf{x}_8 \tag{39}$$

where $\mathbf{C}_8$ is the transform matrix as defined in (36), $\mathbf{x}_8$ and $\mathbf{X}_8$ are the input data and transformed column vectors, respectively. Firstly, the row vectors of $\mathbf{C}_8$ are rearranged through a conversion of the bit reversal and converted Gray code [11]. The example for such conversion for $N = 8$ is tabulated in Table VIII. Therefore, (39) becomes

$$\mathbf{P}\mathbf{X}_8 = \mathbf{P}\mathbf{C}_8 \mathbf{x}_8 \tag{40}$$

where $\mathbf{P}$ is a permutation matrix which provides the arrangement of the row vectors of $\mathbf{C}_8$ as mentioned in Table VIII.

TABLE VIII: CONVERSION THROUGH A BIT REVERSAL AND CONVERTED GRAY CODE ($N = 8$).

Decimal	Binary	Bit Reversal	Converted Gray Code	Decimal
0	000	000	000	0
1	001	100	111	7
2	010	010	011	3
3	011	110	100	4
4	100	001	001	1
5	101	101	110	6
6	110	011	010	2
7	111	111	101	5

Therefore,

$$\mathbf{C}_P = \mathbf{P}\mathbf{C}_8 = \begin{bmatrix} 1 & 1 & 1 & 1 & 1 & 1 & 1 & 1 \\ 1 & -1 & 1 & -1 & 1 & -1 & 1 & -1 \\ 0 & 1 & 0 & -1 & 0 & 1 & 0 & -1 \\ 1 & 0 & -1 & 0 & 1 & 0 & -1 & 0 \\ 0 & 0 & 1 & 1 & 0 & 0 & -1 & -1 \\ 0 & 0 & -1 & 1 & 0 & 0 & 1 & -1 \\ 1 & 1 & 0 & 0 & -1 & -1 & 0 & 0 \\ 1 & -1 & 0 & 0 & -1 & 1 & 0 & 0 \end{bmatrix}. \tag{41}$$

For simplicity, the scaling factor diagonal matrix $\mathbf{D}_8$ is omitted in the above expression and the subsequent derivation. Now let us focus on the factorization of the matrix in (41) to derive the fast algorithm. $\mathbf{C}_P$ can be rewritten and factorized as

$$\mathbf{C}_P = \begin{bmatrix} \mathbf{C}_4 & \mathbf{C}_4 \\ \mathbf{C}'_4 & -\mathbf{C}'_4 \end{bmatrix} = \begin{bmatrix} \mathbf{C}_4 & \mathbf{0} \\ \mathbf{0} & \mathbf{C}'_4 \end{bmatrix} \begin{bmatrix} \mathbf{I}_4 & \mathbf{I}_4 \\ \mathbf{I}_4 & -\mathbf{I}_4 \end{bmatrix} \tag{42}$$

where

$$\mathbf{C}_4 = \begin{bmatrix} 1 & 1 & 1 & 1 \\ 1 & -1 & 1 & -1 \\ 0 & 1 & 0 & -1 \\ 1 & 0 & -1 & 0 \end{bmatrix}, \mathbf{C}'_4 = \begin{bmatrix} 0 & 0 & 1 & 1 \\ 0 & 0 & -1 & 1 \\ 1 & 1 & 0 & 0 \\ 1 & -1 & 0 & 0 \end{bmatrix}.$$

Equation (42) can be further factorized as

$$\mathbf{C}_P = \begin{bmatrix} \mathbf{C}_2 & \mathbf{C}_2 & & \\ \hat{\mathbf{I}}_2 & -\hat{\mathbf{I}}_2 & & \\ & & \mathbf{0} & \mathbf{C}'_2 \\ & & \mathbf{C}_2 & \mathbf{0} \end{bmatrix} \begin{bmatrix} \mathbf{I}_4 & \mathbf{I}_4 \\ \mathbf{I}_4 & -\mathbf{I}_4 \end{bmatrix} \tag{43}$$

where

$$\mathbf{C}_2 = \begin{bmatrix} 1 & 1 \\ 1 & -1 \end{bmatrix}, \mathbf{C}'_2 = \begin{bmatrix} 1 & 1 \\ -1 & 1 \end{bmatrix} \text{ and } \hat{\mathbf{I}}_2 = \begin{bmatrix} 0 & 1 \\ 1 & 0 \end{bmatrix}.$$

Finally, we have

$$\mathbf{C}_P = \begin{bmatrix} \mathbf{C}_2 & & & \\ & \hat{\mathbf{I}}_2 & & \\ & & \mathbf{C}'_2 & \\ & & & \mathbf{C}_2 \end{bmatrix} \begin{bmatrix} \mathbf{I}_2 & \mathbf{I}_2 & & \\ \mathbf{I}_2 & -\mathbf{I}_2 & & \\ & & \mathbf{0} & \mathbf{I}_2 \\ & & \mathbf{I}_2 & \mathbf{0} \end{bmatrix} \cdot \begin{bmatrix} \mathbf{I}_4 & \mathbf{I}_4 \\ \mathbf{I}_4 & -\mathbf{I}_4 \end{bmatrix} \tag{44}$$

which results in fast forward algorithm after substituting it into (40). The output sequence is needed to be rearranged according to the permutation matrix $\mathbf{P}$. The signal flow graph for the fast forward algorithm is illustrated in Fig. 7.

REFERENCES

[1] C. M. Mak, C. K. Fong, and W. K. Cham, "Fast motion estimation for H.264/AVC in Walsh-Hadamard domain," *IEEE Trans. Circuits and Systems for Video Technology*, vol. 18, no. 6, pp. 735–45, 2008.

[2] I. Valova and Y. Kosugi, "Hadamard-based image decomposition and compression," *IEEE Transactions on Information Technology in Biomedicine*, vol. 4, no. 4, pp. 306–319, 2000.

[3] C. F. Chan, "Efficient implementation of class of isotropic quadratic filters by using Walsh-Hadamard transform," *Electronics Letters*, vol. 35, no. 16, pp. 1306–1308, 1999.

[4] W. S. Liao, B. S. Lin, B. S. Lin, H. D. Wu, and F. C. Chong, "Ambient noise canceller in pulmonary sound using WHT transform domain adaptive filter," in *IEEE 24th Annual International Conference of the Engineering in Medicine and Biology Society*, vol. 1, Houston, TX, USA, 2002, pp. 86–7.

[5] S. H. Tsai, Y. P. Lin, and C. C. J. Kuo, "MAI-free MC-CDMA systems based on Hadamard-Walsh codes," *IEEE Transactions on Signal Processing*, vol. 54, no. 8, pp. 3166–79, 2006.

[6] R. S. Stankovic, "Some remarks on terminology in spectral techniques for logic design: Walsh transform and Hadamard matrices," *IEEE Transactions on Computer-Aided Design of Integrated Circuits and Systems*, vol. 17, no. 11, pp. 1211–1214, 1998.

[7] L. Zhang, Z. H. Lin, and Z. W. Lv, "Technology mapping and Hadamard transform," in *IEEE Int. Conf. on Communications, Circuits and Systems and West Sino Exposition*, China, 2002, pp. 1381–1385.

[8] R. Yarlagadda and J. Hershey, *Hadamard matrix analysis and synthesis with applications to communications and signal/image processing*. Norwell, MA: Kluwer, 1997.

[9] B. Arambepola and K. Partington, "Walsh-Hadamard transform for complex-valued signals," *Electron. Lett.*, vol. 28, no. 3, pp. 259–61, 1992.

[10] L. Zhihua and Z. Qishan, "Ordering of Walsh functions," *IEEE Trans. Electromagnetic Compatibility*, vol. EMC-25, no. 2, pp. 115–19, 1983.

[11] K. G. Beauchamp, *Applications of Walsh and related functions, with an introduction to sequency theory*. Academic Press, 1984.

[12] C. K. Yuen, "Remarks on the orderings of Walsh functions," *IEEE Transactions on Computers*, vol. C-21, no. 12, p. 1452, 1972.

[13] H. F. Harmuth, "A generalized concept of frequency and some applications," *IEEE Trans. Information Theory*, vol. IT-14, no. 3, pp. 375–382, 1968.

[14] B. Bhagavan and R. Polge, "Sequencing the Hadamard transform," *IEEE Trans. Audio and Electroacoustics*, vol. 21, no. 5, pp. 472–473, 1973.

[15] S. Rahardja and B. J. Falkowski, "Family of Unified Complex Hadamard Transforms," *IEEE Transactions on Circuits and Systems II-Analog and Digital Signal Processing*, vol. 46, no. 8, pp. 1094–1100, 1999.

[16] ——, "Complex composite spectra of unified complex Hadamard transform for logic functions," *IEEE Trans. Circuits and Systems II-Analog and Digital Signal Processing*, vol. 47, no. 11, pp. 1291–1297, 2000.

[17] S. Xie and S. Rahardja, "Performance evaluation for quaternary DS-SSMA communications with complex signature sequences over Rayleigh-fading channels," *IEEE Transactions on Wireless Communications*, vol. 4, no. 1, pp. 266–77, 2005.

[18] A. Aung, B. P. Ng, and S. Rahardja, "Sequency-ordered complex Hadamard transform: Properties, computational complexity and applications," *IEEE Trans. Signal Process.*, vol. 56, no. 8, pp. 3562–71, 2008.

[19] ——, "Performance of SCHT sequences in asynchronous CDMA system," *IEEE Communications Letters*, vol. 11, no. 8, pp. 641–3, 2007.

[20] K. J. R. Liu, "A simple and unified proof of dyadic shift invariance and the extension to cyclic shift invariance," *IEEE Transactions on Education*, vol. 36, no. 4, pp. 369–72, 1993.

[21] G. Bi, A. Aung, and B. P. Ng, "Pipelined hardware structure for sequency-ordered complex Hadamard transform," *IEEE Signal Processing Letters*, vol. 15, pp. 401–4, 2008.

[22] J. G. Proakis and D. G. Manolakis, *Digital signal processing: Principles, algorithms, and applications*, 4th ed. Pearson Prentice Hall, 2007.

[23] N. N. Ponomarenko, K. O. Egiazarian, V. V. Lukin, and J. T. Astola, "High-quality DCT-based image compression using partition schemes," *IEEE Signal Processing Letters*, vol. 14, no. 2, pp. 105–108, 2007.

[24] M. Puschel and J. M. F. Moura, "Algebraic signal processing theory: Cooley-Tukey type algorithms for DCTs and DSTs," *IEEE Transactions on Signal Processing*, vol. 56, no. 4, pp. 1502–1521, 2008.

[25] R. C. Gonzalez and R. E. Woods, *Digital image processing*, International ed. Pearson Prentice Hall, 2002.

[26] N. Ahmed, K. R. Rao, and A. L. Abdussattar, "BIFORE or Hadamard transform," *IEEE Trans. Audio, Electroacoustics*, vol. AU-19, no. 3, pp. 225–34, 1971.

Aye Aung received the B.Eng. degree in electrical and electronic engineering from the Nanyang Technological University (NTU), Singapore, in 2005. Since 2006, he has been working towards the Ph.D. degree at NTU, Singapore.

His research interests include digital signal processing for multimedia applications and communications, signal analysis and synthesis, fast algorithms for various transforms, image signal processing in general, multimedia digital watermarking, and wireless communications.

Boon Poh Ng received the B.Eng. degree in electrical engineering from the Nanyang Technological Institute, Singapore, in 1987, the D.I.C. and M.Sc. degrees in communications and signal processing from the Imperial College, University of London, London, U.K., in 1991, and the Ph.D. degree from the Nanyang Technological University (NTU), Singapore, in 1995.

He was a Lecturer with the Department of Electronics and Communication Engineering, Singapore Polytechnic, from 1987 to 1996. From 1996 to 1999, he was a Senior Research Fellow at the Centre for Signal Processing, NTU. He is currently an Associate Professor at the School of Electrical and Electronic Engineering, NTU. His research interests include array synthesis, adaptive array processing, spectral estimation, and digital signal processing in general.

Dr. Susanto Rahardja received his B.Eng. degree from the National University of Singapore, and M.Eng. and Ph.D. degrees from the Nanyang Technological University (NTU, Singapore), all in Electrical & Electronic Engineering. He is currently the Director of Personal 3D Entertainment System program and Head of Signal Processing department at the Institute for Infocomm Research (IR). He is also a program director of Infuse initiative at Science and Engineering Research Council (SERC) of A*STAR. His research interests are in Audio/Video Signal Processing, Image Processing, Spread Spectrum and Multi-user Detection Techniques for CDMA Applications, Digital Signal Processing Algorithms and Implementations, of which he has more than 200 publications in internationally refereed journals and conferences.

Dr Rahardja is an Associate Professor at the School of Electrical and Electronic Engineering in NTU and a Senior Member of the Institute of Electrical and Electronics Engineers (IEEE). He was the recipient of the IEE Hartree Premium Award in 2002. In 2003, Dr Rahardja received the prestigious Tan Kah Kee Young Inventors' Gold award in the Open Category, for his contributions on scalable to lossless audio compression technology.

Since 2002, Dr Rahardja actively participated in the international ISO/IEC JTC1/SC29/WG11 (Moving Picture Expert Group, or MPEG) where he contributed to MPEG-4 Scalable to Lossless System (SLS) and the technology is incorporated and published in ISO/IEC 14496-3:2005/Amd.3:2006. He also contributed technology to the MPEG-4 Audio Lossless System (ALS) where it is now incorporated in ISO/IEC 14496-3:2005/Amd.2:2006. In recognition for his contributions to the national standardization program, Dr Rahardja was awarded the Standards Council Merit Award by SPRING Singapore in 2006. For his leadership and technical contribution to advancement of digital audio signal processing and its adoption to the MPEG, he was awarded the National Technology Award in 2007.

Dr Rahardja has served in several boards, advisory and technical committees in various IEEE and SPIE as well as ACM SIGGRAPH related professional activities in the areas of multimedia. He is elected members of the Technical Committee of the Visual Signal Processing and Communications, Circuits and Systems for Communications and Multimedia Systems and Applications of the IEEE Circuits & Systems Society. He is currently serving as Associate Editors for IEEE Transactions on Audio, Speech and Language Processing and IEEE Transactions on Multimedia as well as the Journal of Visual Communication and Image Representation. He received the A*STAR Most Inspiring Mentor Award in March 2008.